Analyst

PAPER

View Article Online
View Journal

Cite this: DOI: 10.1039/c9an02051a

Target-activated DNA nanomachines for the ATP detection based on the SERS of plasmonic coupling from gold nanoparticle aggregation†

Yanfang Cui,[a] Haiwang Wang,[b] Su Liu,[c] Yu Wang *[a] and Jiadong Huang [a,d]

The self-assembly of plasmonic nanoparticles provides a powerful approach to generate surface-enhanced Raman scattering (SERS), which promotes the actual applications in chemical and biomolecular analyses. Herein, we developed a facile SERS sensing strategy for an ATP assay with a 3-D DNA nanomachine that walks by the Exo III cleavage, leading to the formation of AuNP aggregates, which resulted in the enhancement of the electromagnetic field. Depending on the target-activated Exo III cleavage, the 3-D nanomachine can walk along the 3-D track on the surface of AuNPs and generate self-assembled hot-spots to enhance the SERS signal of a Raman dye, allowing a homogenous assay of the ATP concentration with high sensitivity and reproducibility. Under optimized experimental conditions, the biosensor detected ATP with a widened dynamic range from 1 pM to 1×10^5 pM with a limit of detection of up to 0.29 pM. Hence, the novel strategy provides a useful and practical platform for the SERS assay of ATP with high sensitivity and repeatability. Besides, this platform shows great potential for applications in high-throughput assays for drug screening and clinical diagnostics.

Received 13th October 2019,
Accepted 12th November 2019

DOI: 10.1039/c9an02051a

rsc.li/analyst

1. Introduction

Surface-enhanced Raman scattering (SERS), as we know, is a phenomenon relevant to a high enhancement factor (as high as 10^{14}) of the Raman signals of targets on the surface of metallic nanostructures.[1–5] In addition, Au and Ag nanoparticles usually act as SERS-active substrates because of their surface plasmons,[6,7] in which all the conduction electrons are in the oscillating mode. However, we often choose gold nanoparticles (AuNPs) as the SERS-active substrate for biosensors on account of their biocompatibility and stability.[8–11] Furthermore, SERS can also provide considerable structural information at the molecular level with high sensitivity compared with fluorescence.[12,13] Recently, some kinds of well-behaved biosensors have been reported based on SERS.[14–16]

Basically, the principle for the SERS is dependent on the local electric field enhancement ("hot-spots") by a dimer of metallic nanoparticles.[17,18] So, it is the key step to reduce the space between two metallic nanoparticles to produce "hot-spots" and enhance the signal of Raman reporters modified on the surface of the substrate.[19] A major challenge in this step is to precisely control the aggregation of the metallic nanoparticles to produce "hot-spots" along a designated path.[20] The rational construction of a self-assembled DNA based on the Watson–Crick base pairing provides a powerful strategy to meet this challenge. Lim *et al.* utilized the dsDNA self-assembly to monitor the space between Au nanoparticles to demonstrate how the SERS signals correlate with the interparticle spacing.[21] This indicated that we can obtain strong Raman signals of the dye modified on the surface of metallic nanoparticles *via* removing the protection of DNA linked to AuNPs by the Au–S bonds and lead to aggregation.

In addition, depending on the specific programmable, facile synthesis and fine biocompatibility, some one- and two-dimensional DNA machines were constructed based on DNA molecules.[22,23] However, most of these DNA machines moved randomly on a micrometer space, which cannot be precisely controlled. It is urgent to construct a 3-D DNA molecule machine to confine the movement of DNA machines to a 3-D track with a nanometer precision. Therefore, Li *et al.* supplied a 3-D DNA walker built from DNA-functionalized gold nanoparticles and achieved the detection of the target *via* fluo-

[a]Department of Clinical Laboratory, Binzhou Medical University Hospital, Binzhou 256603, P. R. China. E-mail: bio_wangy@ujn.edu.cn; Fax: +86-531- 82769122; Tel: +86-531-89736122
[b]College of Biological Sciences and Technology, University of Jinan, Jinan 250022, P. R. China
[c]College of Water Conservancy and Environment, University of Jinan, Jinan 250022, P. R. China
[d]Key Laboratory of Chemical Sensing & Analysis in Universities of Shandong, College of Chemistry and Chemical Engineering, University of Jinan, Jinan 250022, P. R. China

†Electronic supplementary information (ESI) available. See DOI: 10.1039/c9an02051a

rescence.[24] Le *et al.* designed a DNA-functionalized AuNP nanomachine to detect proteins or nucleic acids based on binding-induced targets.[25] These strategies involve the enzymatic cleavage reaction to drive the nucleic acid strand to move autonomously along the AuNP surface until all the cleavages are complete and the nanomachine stops. Furthermore, aptamers are a class of nucleic acids, which are separated *via* the *in vitro* systematic evolution of ligands by exponential enrichment (SELEX).[26] Aptamers possess properties such as high chemical stability that are satisfactory and can be chemically synthesized in an inexpensive and reproducible way.[27] Upon binding of small molecules with their aptamers, the target can induce a specific event that activates nanomachines used in biosensors. In addition, aptamers generally have higher affinity for their target molecules than the partly complementary DNA, so we can use the target to start the reaction.[28]

Based on the above-mentioned principles, we construct a biosensor based on target-induced DNA nanomachines for the highly sensitive detection of biomolecules using the package of aptamer-based lock design with the SERS technology. As demonstrated, we chose adenosine triphosphate (ATP), which is a major source of energy and plays a key role in cellular metabolism, synthesis and biochemical pathways, as a target biomolecule to confirm the feasibility of our design.[29] As illustrated in Scheme 1, our DNA nanomachine is constructed with AuNPs modified with a Raman dye and three types of nucleic acid strands on the surface. First, the 5′ terminus of the DNA walker strand (DWS) was fixed on the surface of AuNPs by an Au–S bond, and its 3′ terminus was locked by an anti-ATP aptamer (Apt) *via* the partial hybridization of DNA. It is a key step in the hybridization process to enhance the signal-to-background ratio and the sensitivity of detection. Second, the DNA track strand (DTs) was also immobilized on the surface of AuNPs by an Au–S bond at the 5′ terminus and was designed to have a partial complementary sequence with DWs. Third, exonuclease III (Exo III) could specifically cleave the DTs in the 3′ to 5′ direction after the formation of a duplex between DWs and DTs because the recessed 3′ termini of DTs was designed earlier.[30,31] Lastly, DWs were able to walk along the 3-D track by Exo III cleaving the DTs at each step. As a result, AuNPs lose the protection of the DNA on the surface after cleavage by Exo III and aggregate with each other under the condition of high salt concentration. The aggregation of AuNPs will provide "hot-spots" to enhance the intensity of SERS of the Raman dye on the surface of the AuNPs. Therefore, we can establish a quantitative relationship between the intensity of SERS and the concentration of the input target.

2. Materials and methods

2.1. Materials and reagents

The oligonucleotides used in this work were HPLC-purified and synthesized by Sangon Biotechnology Co. Ltd (Shanghai, China). The sequences of the synthesized oligonucleotides are given in Table 1.

Phosphine hydrochloride was purchased from Aladdin (Shanghai, China). Chloroauric acid ($HAuCl_4{\cdot}4H_2O$) and trisodium citrate were acquired from Shanghai Reagent Company (Shanghai, China). Phosphate buffer (PB, 100 mM, pH = 7.4) and phosphate-buffered saline (PBS, contains PB, 10 mM, NaCl, 2 M, pH = 7.4) were purchased from Aladdin (Shanghai, China). Exonuclease III (Exo III), Shrimp Alkaline Phosphatase (SAP), ATP, ADP, GTP, CTP and UTP were purchased from New England Biolabs (Ipswich, MA, USA). The Raman-active dye of 4-nitrothiophenol (4-NTP) was purchased from Sigma Aldrich

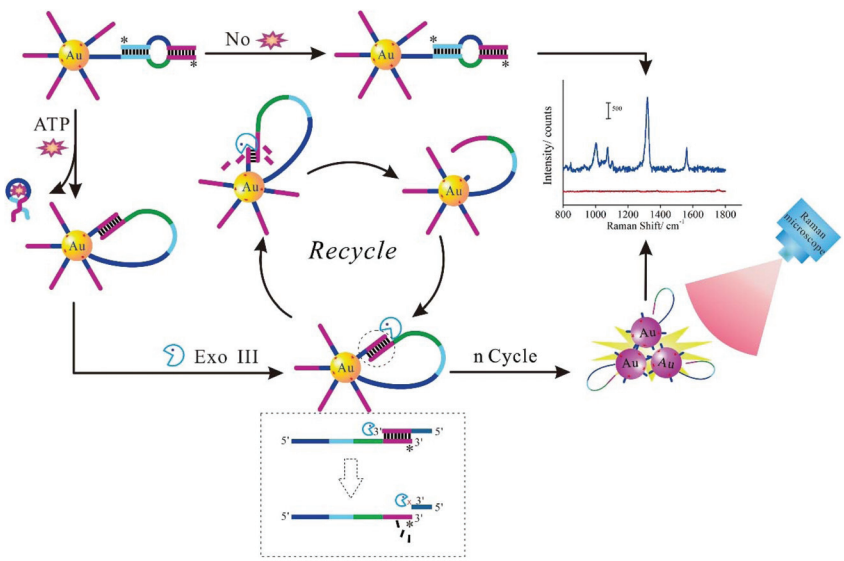

*shows the phosphorothioate modification of last three bases

Scheme 1 Schematic of the DNA nanomachine for the SERS assay of the ATP-based on target-activated plasmonic coupling. *Shows the phosphorothioate modification of last three bases.

Table 1 Synthesized oligonucleotides used in the experiments[a]

Name	DNA sequences (from 5′ to 3′)
DWs	SH-TTTT TTTT TTTT TTTT TTTT TTTT ACCT TCCT TTTTTT CCCC AG*G*T*
DTs	SH-TTTTACCTGGGG
Apt	ACCTGGGGGAGTATTGCGGAGGAAG*G*T*
Apt control	ACCTGGCCATTATACGGCCAGGAAG*G*T*

[a] The asterisk show the phosphorothioate modification of the bases.

Corporation (St Louis, MO, USA). All other reagents were of analytical reagent grade and were used directly without further purification. Ultrapure water used in all experiments was obtained from a Millipore filtration system.

2.2. Apparatus

Absorption spectra were recorded using a UV2600 UV-vis spectrophotometer (Shimadzu international trading Co. Ltd, Japan) at room temperature. Transmission electron microscopy (TEM) measurements were recorded using a JEM-3010 transmission electron microscope. The samples for TEM characterization were prepared by adding a drop of AuNP solution onto a carbon-coated copper grid and drying it at room temperature. Dynamic light scattering (DLS) analysis was performed using a Malvern Zetasizer 3000 HS particle size analyzer (Malvern Instruments, UK). SERS spectra were recorded using a Raman spectrometer (Horiba HR Evolution 800) at a laser wavelength of 633 nm.

2.3. Preparation of the DNA nanomachines with AuNP-modified DNA

Gold nanoparticles were prepared *via* the citrate reduction of $HAuCl_4$ according to a documented protocol.[32] Briefly, 3 mL 1% (w/w) sodium citrate was quickly added to 200 mL boiling solution of 0.01% (w/w) $HAuCl_4$ and kept boiling for 20 min after the solution changed from blank to wine red, ensuring complete reduction. Then, it was slowly cooled to room temperature after the removal of a heat source. The size of the obtained gold nanoparticles is about 20 nm and the concentration is about 0.3 nM based on the extinction coefficient of 2.8×10^9 M^{-1} cm^{-1} at 528 nm. The products were stored at 4 °C before use.

Then, 40 μM thiolated DWs were first hybridized with equal amounts of Apt *via* an annealing process in a buffer solution containing 1× PBS (200 mM NaCl, pH 7.4) at 95 °C for 5 min, followed by slow cooling to room temperature, forming a duplex structure.

Detection probe- and Raman-active dye-modified gold nanoparticles were prepared according to a previously reported protocol.[24,33] Briefly, the AuNP solution (1 mL) was centrifuged at 12 000 rpm for 15 min and redispersed in ultrapure water (300 μL). Two aliquots of the dye solution (50 μM, 12 μL) and mixed nucleic acid solution (150 μL solution containing 2.5 μM mixed solution of DWs and Apt and 50 μM DTs) were added into the above concentrated AuNP solution under magnetic stirring. After reaction for 24 h at 4 °C, the mixture was added slowly to a 50 μL phosphate buffer (PB, 100 mM, pH 7.4) and 27 μL PB saline (PBS, 10 mM, pH 7.4, 2 M NaCl) for another 48 h under 4 °C. Finally, the mixture solution was slowly added to 62 μL PBS with 0.3 M NaCl and kept at 4 °C for further 24 h. The unmodified Raman-active dye and nucleic acid were removed *via* centrifugation at 12 000 rpm for 15 min. Then, the sediment was re-suspended in 1 mL ultrapure water. This step was repeated three times to completely remove excess Raman-active dye and nucleic acid. Subsequently, the AuNP modified with Raman-active dye and nucleic acid probe was re-dispersed in 300 μL ultrapure water and stored at 4 °C until use. The final concentration of the modified AuNP solution is ~1 nM, not considering the loss of AuNPs during the preparation process.

2.4 Activity detection of ATP-based SERS by AuNP aggregation

The detection of ATP includes two continuous steps. First, 10 μL modified AuNP solution was added into the reaction system (20 μL) containing different concentrations of ATP, 5 U Exo III, and 2 μL 10× NEB buffer 2 and incubated at 37 °C for 60 min. Then, the reaction solution was immediately subjected to SERS measurements on a silicon wafer using a confocal Raman system equipped with a 633 nm He–Ne laser.

2.5 Detection of ATP in biological samples

The serum samples were obtained by the centrifugation of whole blood after coagulation.[34] Then, we added different concentrations of ATP (0, 10 pM, 100 pM, and 1 nM) into the human serum samples and measured without any further procedure involved except for dilution with a buffer solution (1 : 10 dilution of serum with buffer). The clinical serum samples used herein were obtained from the University of Jinan Hospital under the prior approval from serum donors. All experiments were performed in accordance with the Guidelines "Standard Operating Procedures of Hospital" and approved by the ethics committee at the "University of Jinan Hospital". Informed consents were obtained from human participants of this study.

3. Results and discussion

3.1 Principle of the design for the ATP concentration assay

Scheme 1 illustrates the working strategy of the designed DNA nanomachine. The DNA nanomachine was constructed with AuNPs modified with the Raman dye and three kinds of nucleic acid strands on the surface. First, the 5′ terminus of the DNA walker strand (DWs) and DNA track strand (DTs) were fixed on the surface of AuNPs by an Au–S bond, and the 3′ terminus of DWs is locked with an anti-ATP aptamer (Apt) *via* the partial hybridization of DNA. This is a key step in the hybridization process to enhance the signal-to-background ratio and the sensitivity of detection. In addition, the three bases at the 3′ terminus of DWs and Apt were subjected to phosphorothio-

ate modification avoiding the digestion of exonuclease III (Exo III) in the reaction solution. In the absence of ATP, there was insignificant SERS signal for the dispersive nanomachine because of the very finite electromagnetic enhancement of individual AuNPs. In the presence of ATP, the target ATP will combine with its aptamer with high specificity, inducing the DWs released from the duplex structure to initiate the nanomachine. The liberated DWs will hybridize with DTs at the 3′ terminus forming the blunt end, which could be digested with Exo III from 3′ to 5′ of the DTs of duplex until DWs were released again (enlarged in the schematic in dotted box). Subsequently, the DWs were able to walk along the 3-D track by Exo III cleaving the DTs at each step. As a result, the AuNPs will lose the protection of the DNA on the surface after Exo III cleaved and aggregate with each other under the condition of high salt environment. The aggregation of the AuNPs yielded uniformly distributed "hot-spots", which significantly enhanced the SERS signal of the Raman dye due to the extremely powerful electromagnetic field. In general, the aggregation of plasmonic nanoparticles is induced by a target-activated nanomachine with Exo III assistance, producing controllable self-assembled "hot-spots" with uniform distribution, narrow electromagnetic field, and equivalent interparticle spacing. Hence, the designed DNA nanomachine might provide a rapid and facile tool for a highly sensitive and specific SERS assay of the ATP with perfect reproducibility.

3.2 Feasibility of the design for the ATP concentration assay

In order to enhance the signal-to-noise ratio and eliminate the interference of the background fluorescence of our design, we selected a non-fluorescent Raman dye, namely 4-NTP, as an SERS reporter. The feasibility of our biosensor was validated under different control conditions for the SERS measurement. As shown in Fig. 1, there was an obvious difference in the SERS signal intensity between the positive and other negative conditions. The distinct SERS signal with a characteristic peak at 1327 cm^{-1} of the Raman dye was obtained in the positive control experiment (curve a), testifying that ATP triggered the DNA nanomachine upon cleavage by Exo III and generated self-assembled hot-spots to enhance the signal intensity. In contrast, in the blank control (curve d), there was no SERS signal observed, indicating that AuNPs modified with DNA were well dispersed and no hot-spots were generated. Similarly, in the other negative control, where the AuNP-modified DNA was incubated only with the target ATP (curve b), no SERS signal was produced either. This suggested that the coordinate interaction of the enzyme is necessary to drive the DNA nanomachine and induce the aggregation of AuNPs. In the end, there were no distinct SERS signals after we used non-aptamers (Apt control) of ATP as blocking nucleic acids of DWs, demonstrating that ATP cannot bind with the blocking nucleic acid. All above information uncover the designed strategy with the potential of being a facile, fast, and low-priced assay method for the highly sensitive SERS detection of ATP concentration.

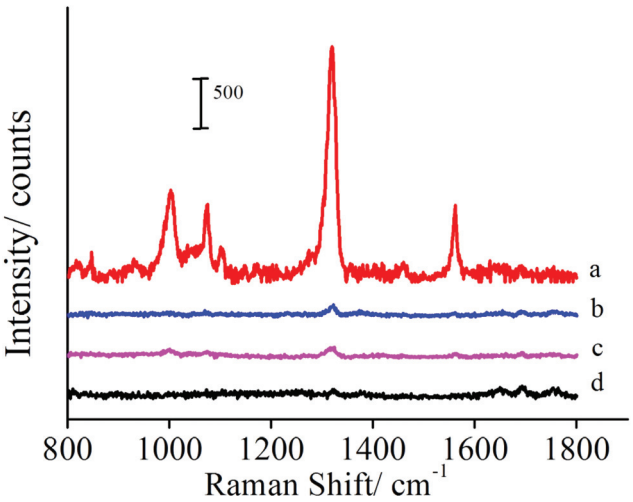

Fig. 1 SERS spectra of control experiments in the ATP concentration assay: the positive sample (curve a), the blank sample (curve d), AuNPs modified with DNA incubated with ATP (curve b) or with Exo III (curve c).

3.3 Characterization of the design for the ATP concentration assay

As this biosensor was based on the aggregation of AuNPs to enhance the SERS signal of the Raman dye, UV-vis absorption and DLS analyses were performed to further testify the mechanism of the biosensor. Fig. 2A describes the special absorption spectral responses of the naked and modified AuNPs. As shown in Fig. 2A, the synthetic naked AuNPs (curve a) and modified AuNPs (curve b) were well dispersed in an aqueous solution with a single absorption peak at 524 nm and 529 nm, respectively. It suggested that the DNA and Raman substrates were successfully modified on the surface of AuNPs by an Au–S bond. Fig. 2B depicts the UV-vis absorption spectra of this strategy with and without the target ATP. We easily found that there was only a strong absorption peak at 530 nm for the blank sample (curve a); however, there was an apparent decline in the absorption intensity at 530 nm accompanied by a new peak at ~700 nm for the positive solution (curve b). Moreover, an obviously red-to-purple color change was observed with naked eyes, indicating the formation of AuNP aggregates because of the target-activated DNA nanomachine with the Exo III cleavage on AuNPs.

In addition, we also confirmed our design with DLS measurements and the results are depicted in Fig. 2C. As shown in Fig. 2C, the average hydrodynamic diameter of modified AuNPs with DNA and Raman dye was ~31.71 nm for the blank sample. In comparison, the average diameter of the positive sample reached ~532.06 nm, indicating the formation of AuNP aggregates, resulting from the target ATP triggering the DNA nanomachine. Beyond that, the design was further validated using TEM to test the morphology of AuNPs in the absence (left) and presence (right) of ATP, and the results are shown in Fig. S1.† Without ATP in the reaction solution, the modified AuNPs with nucleic acids and Raman dye could be

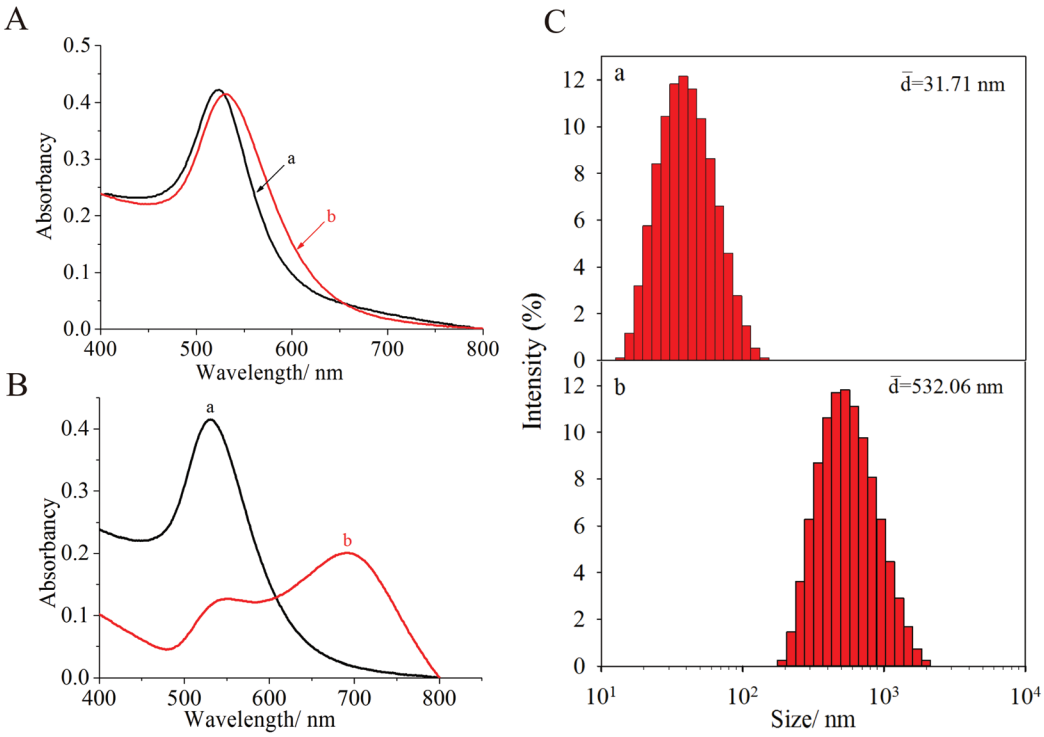

Fig. 2 (A) UV absorption spectra of naked AuNPs (a) and AuNPs modified with DNA and Raman dye (b). (B) The UV absorption spectral of modified AuNPs incubated with Exo III in the absence (a) and presence (b) of ATP. (C) Diameter distribution of the modified AuNPs incubated with Exo III in the absence (a) and presence (b) of ATP.

homogenously dispersed in the reaction solution, and there was no apparent aggregation between the AuNPs. After addition into the reaction solution, ATP can specifically recognize its aptamer, which locked the DWs. Then, the DWs will hybridize with DTs at the 3′ terminus forming the blunt end, which could be digested with Exo III from 3′ to 5′ of DTs of the duplex. After multiple cycles, the DTs modified on the AuNPs will be digested completely by Exo III. Subsequently, there were no adequate nucleic acids on the surface of the AuNPs, and they will form the aggregation because of the high salt concentration in the reaction solution. The smaller distance between adjacent AuNPs will form effective plasmonic coupling that created a strong electromagnetic field within the interparticle gap. All the given data provide powerful evidence that this designed biosensor could be promisingly used for the ATP concentration assay.

3.4 Optimization of experimental conditions

To achieve the optimal analytical performance of the biosensor, some key experimental conditions including reaction time and the concentration of modified AuNPs were investigated. Fig. 3 shows the influence of the reaction time on the signal-to-noise ratio by probing the SERS signal towards 10 nM of ATP (the red curve) and the blank sample (the black curve). As shown in Fig. 3A, the Raman peak intensity at 1327 cm^{-1} increased with the increase in the reaction time, and then reached equilibrium after 60 minutes as compared with the positive sample. Therefore, 60 min was chosen as the optimum reaction time in the following assay. Furthermore, in order to enhance the signal-to-noise ratio of the biosensor, the concentration of modified AuNPs in the reaction solution was investigated, and the result is shown in Fig. 3B. The best signal-to-noise ratio was obtained when the concentration of the modified AuNPs was 0.25 nM. Therefore, 0.25 nM was chosen as the optimal concentration of modified AuNPs in the following assay.

3.5 Specificity of the biosensor

The specificity of the biosensor is a crucial factor for its potential applications in real biological samples. Therefore, in order to testify the specificity of our design for the ATP detection, the experiment was performed using four similar molecules, namely, ADP, GTP, CTP and UTP. Fig. 4 depicts the SERS signal intensity at 1327 cm^{-1} of the biosensor in response to different targets. It was shown that the SERS signal intensity at 1327 cm^{-1} was only due to the presence of ATP, while no obvious SERS signal intensity appeared in other non-target interfering molecules, demonstrating the high selectivity of the strategy for the ATP assay.

3.6 Analytical performance of the DNA nanomachine biosensor for the ATP assay

Under standard procedures and optimized conditions, the analytical performance of the DNA nanomachine biosensor was investigated by the assay of ATP with different concentrations. As shown in Fig. 5, the SERS intensities increased

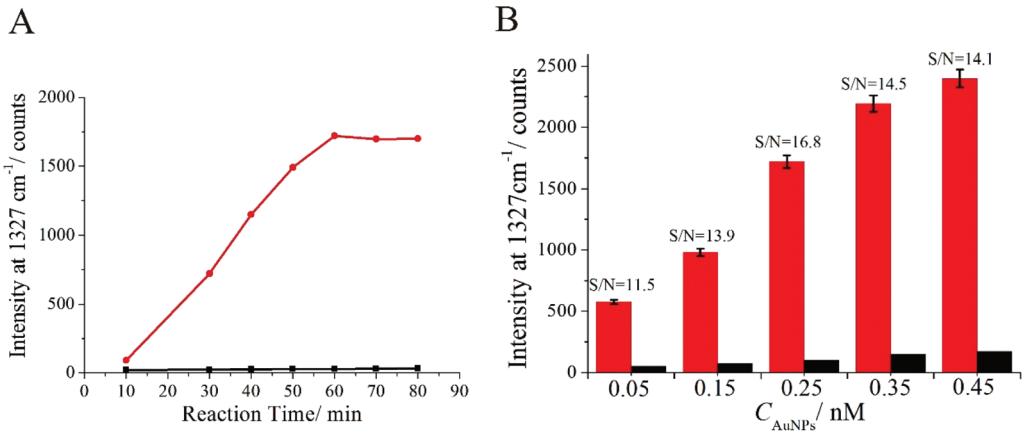

Fig. 3 (A) Effect of the reaction time on the intensity at 1327 cm^{-1}. (B) Effect of the concentration of modified AuNPs on the intensity at 1327 cm^{-1}. The results for both plots were obtained using 10 nM target ATP.

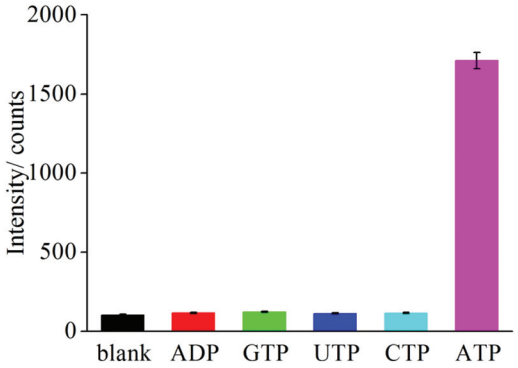

Fig. 4 Specificity evaluation of the biosensor for the ATP concentration assay.

with the increase in the ATP concentration from 0 to 10^5 pM. A linear dependence between the SERS peak intensity and the ATP concentrations was obtained in the range from 1 to 10^5 pM. The limit of detection (LOD) was calculated to be 0.288 pM according to the 3σ rule, which was better than those of previous assays of ATP, and the detailed comparison is shown in Table 2. In addition, the relative standard deviations (RSD) were 2.5%, 1.9%, 2.2%, and 2.3% in four repetitive assays of 0.01, 0.1, 1, and 10 nM of ATP, indicating excellent reproducibility of the DNA nanomachine biosensor because of the target-activated self-assembly of AuNPs. Besides, our concept provided the advantages of fast, low-cost, and facile detection with only one-step operation. Therefore, our DNA nanomachine biosensor can offer a facile and universal platform for a highly sensitive and specific assay of the ATP concentration.

3.7 Real sample analysis

To demonstrate the applicability of the sensing concept for the ATP detection, we applied the biosensor in a complicated biological environment. We directly detected the concentration of ATP in human serum samples. The chemical composition of the serum is similar to that of the plasma except without ATP. Different concentrations of ATP (0, 10 pM, 100 pM and 1 nM) were added into the serum, and the samples were detected

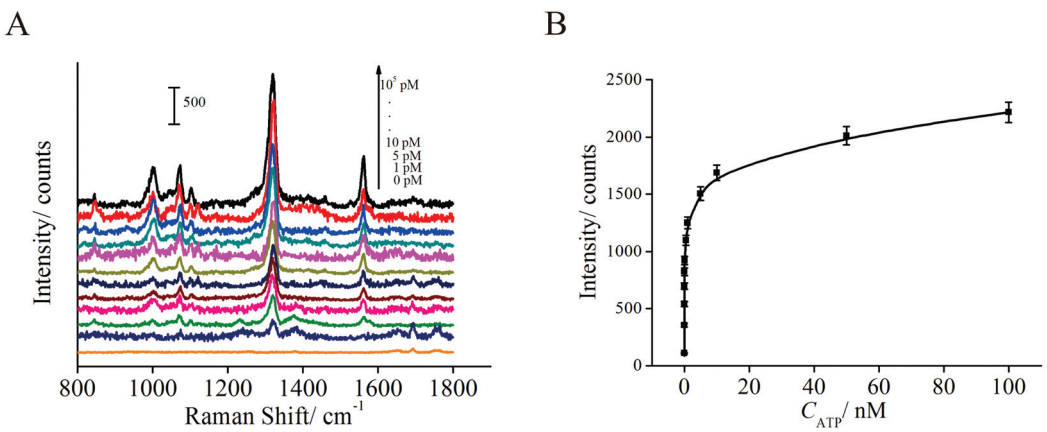

Fig. 5 (A) Plot of SERS spectra in response to ATP at different concentrations. (B) Plot of SERS signal intensities at 1327 cm^{-1} *versus* ATP concentration (the error bars are standard deviations across four repeating tests).

Table 2 Comparison of different assay strategies for ATP concentration

Detection methods	Detection range (pM)	Detection limit (pM)	Ref
Electrochemical	1.0×10^4–1.0×10^9	5.6×10^3	35
Electrochemiluminescent	1.0×10^2–1.0×10^3	2.0×10^1	36
UV-vis	4.4×10^6–1.3×10^8	6.0×10^7	37
Colorimetric and fluorometric	1.0×10^5–5.0×10^6	6.3×10^4	38
Fluorometric	1.0×10^3–1.0×10^4	2.6×10^2	39
SERS	1.0×10^1–1.0×10^4	0.85	40
This work	1.0–1.0×10^5	0.29	

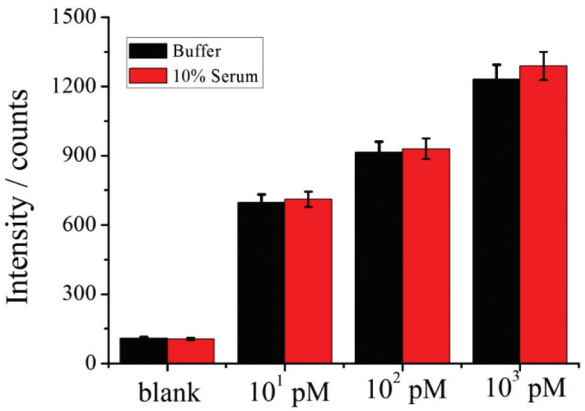

Fig. 6 SERS intensity responses of the biosensing for the ATP detection in buffers (black bar) and human serum samples (red bar). The error bars are standard deviations across four repetitive experiments.

Table 3 ATP analysis in serum samples

Sample	Added amount (pM)	Proposed method (±SD, $n = 4$)
Human serum 1	1.000×10^1	$(1.012 \pm 0.033) \times 10^1$
Human serum 2	1.000×10^2	$(0.963 \pm 0.042) \times 10^2$
Human serum 3	1.000×10^3	$(0.981 \pm 0.028) \times 10^3$

using the biosensor. Fig. 6 shows the clinical results of our system in the reaction solution (black bar) and in the serum sample (red bar). The results demonstrated that the data gained in the human serum were in accordance with those obtained in the buffer, indicating the feasibility of this strategy for real samples with good reliability and accuracy. The specific data of the ATP detection in the serum samples are given in Table 3. The results also demonstrate that the concentration of ATP in a biological environment was in agreement with our sensing method, indicating that the strategy can be applied for the assay of ATP in real samples.

4. Conclusions

In summary, we have developed a facile SERS sensing strategy for an ATP assay with a 3-D DNA nanomachine that walks by the Exo III cleavage leading to the formation of AuNP aggregates, which brought the enhancement of the electromagnetic field. Depending on the target activation and Exo III cleavage, the 3-D nanomachine can walk along the 3-D track on the surface of AuNPs and generate self-assembled hot-spots to enhance the SERS signal of a Raman dye, allowing a homogenous assay of the ATP concentration with high sensitivity and reproducibility. There are two highlights about this strategy, which are as follows: first, we used the anti-ATP aptamer to lock the 3′ terminal of DWs, enhancing the specificity of the biosensor. Second, the novel strategy of the 3-D nanomachine is aided by Exo III, which not only drives the nanomachine moving step by step to offer the SERS signal but also detects ATP with a widened dynamic range from 1 pM to 1×10^5 pM and noteworthy sensitivity, with a limit of detection up to 0.29 pM. Hence, the novel strategy provides a useful and practical platform for the SERS assay of ATP with high sensitivity and repeatability. Besides, this platform also shows great potential to be used in high-throughput assays for drug screening and clinical diagnostics.

Conflicts of interest

There are no conflicts to declare.

Acknowledgements

This work was supported by National Natural Science Foundation of China (31471644), the Primary Research & Development Plan of Shandong Province (2017GSF220009).

References

1 J. F. Li, S. Y. Ding, Z. L. Yang, M. L. Bai, J. R. Anema, X. Wang, A. Wang, D. Y. Wu, B. Ren, S. M. Hou, T. Wandlowski and Z. Q. Tian, *J. Am. Chem. Soc.*, 2011, **133**, 15922–15925.
2 L. V. Brown, K. Zhao, N. King, H. Sobhani, P. Nordlander and N. J. Halas, *J. Am. Chem. Soc.*, 2013, **135**, 3688–3695.
3 N. R. Agarwal, P. M. Ossi and S. Trusso, *Appl. Surf. Sci.*, 2019, **466**, 19–27.
4 S. M. Morton and L. Jensen, *J. Am. Chem. Soc.*, 2009, **131**, 4090–4098.
5 I. Yoon, T. Kang, W. Choi, J. Kim, Y. Yoo, S.-W. Joo, Q. H. Park, H. Ihee and B. Kim, *J. Am. Chem. Soc.*, 2009, **131**, 758–762.
6 M. Rycenga, X. H. Xia, C. H. Moran, F. Zhou, D. Qin, Z. Y. Li and Y. A. Xia, *Angew. Chem., Int. Ed.*, 2011, **50**, 5473–5477.
7 P. Li, M. Ge, L. Yang and J. Liu, *Analyst*, 2019, **144**, 421–425.
8 K. Shin, K. Ryu, H. Lee, K. Kim, H. Chung and D. Sohn, *Analyst*, 2013, **138**, 932–938.
9 Y. Zeng, J.-Q. Ren, A.-G. Shen and J.-M. Hu, *J. Am. Chem. Soc.*, 2018, **140**, 10649–10652.

10 R. M. Jarvis, H. E. Johnson, E. Olembe, A. Panneerselvam, M. A. Malik, M. Afzaal, P. O'Brien and R. Goodacre, *Analyst*, 2008, **133**, 1449–1452.
11 O. Péron, E. Rinnert, T. Toury, M. Lamy de la Chapelle and C. Compère, *Analyst*, 2011, **136**, 1018–1022.
12 A.-I. Henry, B. Sharma, M. F. Cardinal, D. Kurouski and R. P. Van Duyne, *Anal. Chem.*, 2016, **88**, 6638–6647.
13 C. Levene, E. Correa, E. W. Blanch and R. Goodacre, *Anal. Chem.*, 2012, **84**, 7899–7905.
14 X. G. Zhang, Z. G. Dai, S. Y. Si, X. L. Zhang, W. Wu, H. B. Deng, F. B. Wang, X. H. Xiao and C. Z. Jiang, *Small*, 2017, **13**, 8.
15 H. Li, Q. Xu, X. Z. Wang and W. Liu, *Small*, 2018, **14**, 9.
16 T. R. Chung, T. Koker and F. Pinaud, *Small*, 2016, **12**, 5891–5901.
17 S. L. Kleinman, B. Sharma, M. G. Blaber, A. I. Henry, N. Valley, R. G. Freeman, M. J. Natan, G. C. Schatz and R. P. Van Duyne, *J. Am. Chem. Soc.*, 2013, **135**, 301–308.
18 H. Y. Chen, M. H. Lin, C. Y. Wang, Y. M. Chang and S. Gwo, *J. Am. Chem. Soc.*, 2015, **137**, 13698–13705.
19 S. Y. Ding, E. M. You, Z. Q. Tian and M. Moskovits, *Chem. Soc. Rev.*, 2017, **46**, 4042–4076.
20 H. W. Cheng, Z. Skeete, Q. M. Ngo, J. Luo and C. J. Zhong, *Phys. Chem. Chem. Phys.*, 2015, **17**, 28529–28533.
21 D. K. Lim, K. S. Jeon, J. H. Hwang, H. Kim, S. Kwon, Y. D. Suh and J. M. Nam, *Nat. Nanotechnol.*, 2011, **6**, 452–460.
22 P. Yin, H. Yan, X. G. Daniell, A. J. Turberfield and J. H. Reif, *Angew. Chem., Int. Ed.*, 2004, **43**, 4906–4911.
23 M.-Q. He, K. Wang, W.-J. Wang, Y.-L. Yu and J.-H. Wang, *Anal. Chem.*, 2017, **89**, 9292–9298.
24 X. Yang, Y. Tang, S. D. Mason, J. Chen and F. Li, *ACS Nano*, 2016, **10**, 2324–2330.
25 H. Zhang, M. Lai, A. Zuehlke, H. Peng, X. F. Li and X. C. Le, *Angew. Chem., Int. Ed.*, 2015, **54**, 14326–14330.
26 R. Stoltenburg, C. Reinemann and B. Strehlitz, *Biomol. Eng.*, 2007, **24**, 381–403.
27 J. Canoura, Z. Wang, H. Yu, O. Alkhamis, F. Fu and Y. Xiao, *J. Am. Chem. Soc.*, 2018, **140**, 9961–9971.
28 R. E. Armstrong and G. F. Strouse, *Bioconjugate Chem.*, 2014, **25**, 1769–1776.
29 X. Q. Leng, R. G. Li, Y. Wang, Y. P. Wu, Y. Q. Tu, Q. Q. Pei, X. J. Cui, J. D. Huang and S. Liu, *New J. Chem.*, 2018, **42**, 3534–3540.
30 X. Wang, T. Hou, T. Lu and F. Li, *Anal. Chem.*, 2014, **86**, 9626–9631.
31 X. Wang, X. Liu, T. Hou, W. Li and F. Li, *Sens. Actuators, B*, 2015, **208**, 575–580.
32 K. C. Grabar, K. R. Brown, C. D. Keating, S. J. Stranick, S. L. Tang and M. J. Natan, *Anal. Chem.*, 1997, **69**, 471–477.
33 Y. Wang, L.-J. Tang and J.-H. Jiang, *Anal. Chem.*, 2013, **85**, 9213–9220.
34 T. Zhao, C. Lin, Q. Yao and X. Chen, *Talanta*, 2016, **154**, 492–497.
35 L. Lu, J. C. Si, Z. F. Gao, Y. Zhang, J. L. Lei, H. Q. Luo and N. B. Li, *Biosens. Bioelectron.*, 2015, **63**, 14–20.
36 C. Wang, C. Y. C. Huang and W. C. Lin, *Biosens. Bioelectron.*, 2013, **43**, 355–361.
37 D. S. Hsu and S. S. Chen, *J. Chromatogr.*, 1984, **311**, 396–399.
38 C. W. Park, J.-W. Park, S. H. Lee and J. Hwang, *Biosens. Bioelectron.*, 2014, **52**, 379–383.
39 J. Xu and C. Wei, *Biosens. Bioelectron.*, 2017, **87**, 422–427.
40 C. Zhou, Z. Yu, W. Yu, H. Liu, H. Zhang and C. Guo, *Mikrochim. Acta*, 2019, **186**, 251.

